Dedico esta tesis a las mujeres mas importantes en mi vida: Leticia Romo, Ma. Luisa Gonzalez y Gema Romo . . . Y a Jorge, mi mas grande tesoro.

Cynthia Paulinne Romo
New Mexico Institute of Mining and Technology
October, 2014

BACKGROUND - ORIENTED SCHLIEREN ANALYSIS OF SHOCK WAVE PROPAGATION FROM ENCASED AND UNCASED EXPLOSIVES

by

Cynthia Paulinne Romo

Submitted in Partial Fulfillment
of the Requirements for the Degree of
Master of Science in Mechanical Engineering
with Specialty in Explosives Engineering

New Mexico Institute of Mining and Technology
Socorro, New Mexico
October, 2014

ABSTRACT

High speed digital video images of encased and uncased large-scale explosions of Ammonium Nitrate Fuel Oil (ANFO), and Composition C-4 (C-4) at different masses were analyzed using the background oriented schlieren visualization technique. The encased explosions for ANFO and C-4 took place in the form of car bombs and pipe bombs respectively. The data obtained from the video footage were used to produce shock wave radius vs time profiles, as well as Mach number vs shock wave position profiles. The experimentally measured shock wave data for each explosive material were scaled using Sachs' scaling laws to a 1 kilogram charge at normal temperature and pressure. The results of C-4 were compared to literature, while the results of scaled ANFO were compared to each other, and to the results obtained during the uncased detonations. The comparison between the scaled profiles gathered from the encased and uncased detonations resulted in the identification of the relative amount of energy lost due to the fragmentation of the case. The C-4 profiles were compared to those obtained from computational simulations performed via CTH. The C-4 results showed an agreement in the data reported in literature and that obtained using the background-oriented schlieren (BOS) technique, as well as a good overall agreement with the profiles obtained computationally.

Keywords: Ammonium Nitrate Fuel Oil; Background Oriented Schlieren; Car bomb; Composition C-4; Explosive Scaling; Pipe Bomb

SPONSORSHIP

This Project was funded by

The United States Department of Homeland Security

Federal Emergency Management Agency

Under the Homeland Security National Training Program (HSNTP)

Award No. DHS-13-NPD-005-000-01

ACKNOWLEDGMENTS

I would like to thank my research adviser, Dr. Michael Hargather, for his academic guidance. I would also like to express my sincere gratitude to Dr. Van Romero, without whom the completion of this thesis would have not been possible, not only for the academic support and funding, but also for the moral encouragement to accomplish my goals, for his patience, and for believing in my capabilities. Moreover, I would like to thank the last member of my thesis committee, Dr. Seokbin Lim, for his encouragement and insightful comments. I also gratefully acknowledge the assistance of R. Weaver, K. Walsh, P. Johnston, T. Gonzalez, T. Collister, and the Ordnance Technicians from the Energetic Materials Research and Testing Center for facilitating the equipment needed to complete this thesis. Furthermore, I would like to thank my SGDL mates, particularly Owen Rockwell and Mike Shattuck, for assisting me in the field.

I would also like to acknowledge those who helped me keep my sanity through this process. Brittni and Barbara Romero, for the memories I will forever cherish in my heart, and for teaching me that being part of a family has nothing to do with sharing the same DNA. Thanks to Kenia Piotrowski for reminding me that sometimes it is acceptable to laugh at the inappropriate moments of life. Thanks to Estefania Venegas, Laura Martinez, Denisse Orona, Angelica Gonzalez, and Larissa Armendariz, for making my visits home even more special. Tomas Delgado, Eduardo Saenz, Patricia Parra, Estela Rodriguez, Angeles Bonilla, and Judy & Ron Shaw, for believing in me, calming my mother's nerves and encouraging me to never give up when things got tough. Thanks to Cinde, Amber, Cody, Logan, Paige, Brandon, Jon, and Jared for the unpredictable entertainment. And thank you, Nicholas Ahlen, for loving me even when I hated myself, for being such a positive influence on my mental frame, and for not letting me give up when stress took the best of me; this journey was definitively less harsh with you by my side.

Lastly, I would like to thank my family: Abi, for being the role model I needed; Jorge, for keeping my feet on the ground and reminding me that everything would be fine; Gema & Memo, for making sure I had everything I needed to succeed; Cesar & America, for caring about my wellbeing; my dear minions, for making me a better person. And most importantly, I would like to thank Leticia Romo, for being there for me every single day of my life, even when hundreds of miles were in between us. Your unconditional support and encouragement is what motivated me to stand tall and keep going when I felt inadequate; I would have not made it without you by my side. And even if I had, my achievements would not mean anything if I could not share them with you. Thank you for making me the luckiest daughter in the world. I love you, Mamma Mia!

CONTENTS

LIST OF TABLES

LIST OF FIGURES

This thesis is accepted on behalf of the faculty of the Institute by the following committee:

Michael J. Hargather, Advisor

I release this document to the New Mexico Institute of Mining and Technology.

Cynthia Paulinne Romo Date

CHAPTER 1

INTRODUCTION

There have been many methods used to observe and analyze the shock wave created by the detonation of high explosives, including retro-reflective shadowgraph and schlieren visualization techniques [1][2][3][4][5][6]. Being able to visualize the shock wave created after an explosion is important because the data obtained from the shock wave offers key information about the explosive event itself [7]. While the aforementioned methods are effective in certain circumstances, the background oriented schlieren (BOS) technique is useful for both small and large-scale experimentation. The application of background-oriented schlieren at a large scale has been investigated, and its simplicity and effectiveness have made it an attractive alternative for explosives analysis and characterization on a large scale in the field [8][9][10][11]. The analysis of the detonation of encased and uncased large-scale high explosives in the form of improvised explosive devices (IEDs) using the BOS technique is the basis of this research.

IEDs are homemade devices designed primarily to kill, or cause extreme damage to both humans and infrastructure [12]. Some of the most recent terrorism tactics encompass the use of IEDs, vehicles, and different targets containing explosives. These devices were responsible for about 90% of the deaths and injuries on soldiers and civilians in Iraq [13]. Unfortunately, there are countless ways to create an IED, limited only by the imagination of the maker. IEDs vary in potency, since there is no limit on their size, configuration, packaging or delivery. The components needed and instructions on how to build IEDs are readily available, regardless of complexity of the device, making these extremely dangerous and popular weapons [12]. The ingredients to make a homemade explosive (HME) can be found anywhere, and the quantities of these commercially available ingredients will always vary, making the stability of each IED different [14]. IEDs can be concealed in many shapes, including, but not limited to, suitcases, postal mail, toys, cell phones, computers, cigarette boxes, bottles, pressure cookers, pipe bombs, and car bombs [12].

IEDs have been widely used as warfare weapons and in terrorism tactics [12]. When these objects are set off, devastation and chaos become present. Fortunately, the United States can count on trained volunteers and First Responders to attend to these disasters. These men and women risk their lives to keep civilians safe and to make the job of forensic investigators a little easier. It is important to find ways to protect those who protect and serve this country.

The BOS technique benefits the analysis of outdoor tests of the detonation of large scale explosives. This technique is used here to visualize the shock wave propagation, and investigate the outcome of the explosions of two of the aforementioned IEDs: pipe bombs (Figure 1.1) and car bombs (Figure 1.2). These IEDs encase Composition C-4 and Ammonium Nitrate Fuel Oil (ANFO) respectively. The information gathered by this technique is used to calculate the shock wave velocity, Mach number, and peak overpressure of these large-scale explosions. These parameters will help characterize the detonation of encased ANFO via comparison to uncased ANFO detonation, as well as provide a relative amount of energy lost due to fragmentation for encased C-4, which is a well know explosive [11], to support the effectiveness of the BOS method.

Figure 1.1: Left: Unexploded pipe bomb. Right: Exploding pipe bomb

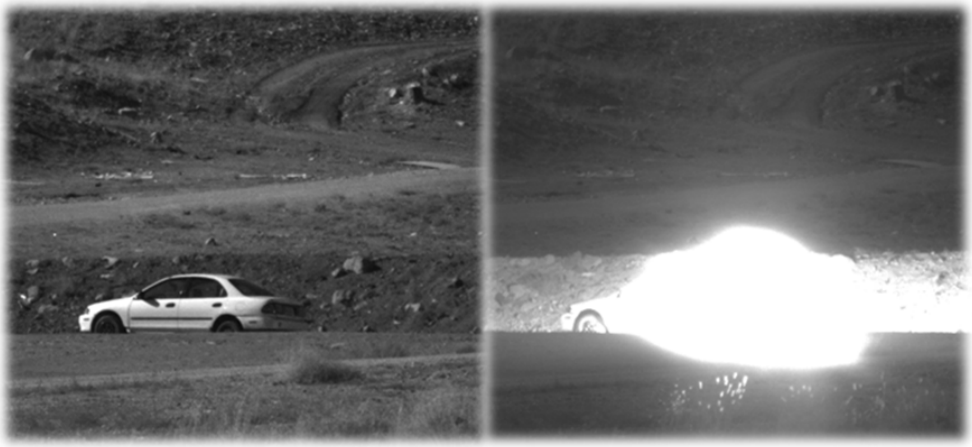

Figure 1.2: Left: Unexploded car bomb. Right: Exploding car bomb

1.1 Energetic Materials

Energetic materials are those materials that release large amounts of energy when undergoing exothermic chemical reactions. Explosives are substances that react chemically almost instantaneously. They produce a rapid evolution of heat and gas, which transfer into an expansion of matter. An explosion can either be mechanical, chemical, or atomic in nature [15]. The events investigated in this work are generated from the initiation of explosives, which results in an exothermic reaction, categorizing these as chemical explosions.

The experiments performed here focused on two main explosive materials, Composition C-4, and Ammonium Nitrate Fuel Oil. Composition C-4 (shown in Figure 1.3) is a solid, yet malleable plastic ideal explosive; its appearance is usually white or light brown, and it is commonly used in military applications [12]. C-4 is the most used putty explosive, a mixture of RDX and a plasticize, in the United States [16]. C-4 is most commonly made out of 91% RDX, 5.3% Di(2ethylhexyl) sebacate, 2.1% Polyisobutylene, and 1.6% oil [17]. Its density can vary from 1.53 to 1.56 g/cm^3 depending on the amount of components the mixture is made out of [16]. C-4 is mainly used in military demolitions, as well as the making of shaped charges, and other special ordnance such as claymore mines [12].

Figure 1.3: Commercial Composition C-4. [12]

Ammonium nitrate is a chemical compound made out of a salt of ammonia and nitric acid; it is commonly used for soil fertilization, but when it is mixed with a fuel, it becomes an explosive [18]. The mixture becomes ammonium nitrate fuel oil (ANFO) which is an industrial explosive, shown in Figure 1.4. ANFO is

typically made out of 94% ammonium nitrate, and 6% fuel oil [17]. The ammonium nitrate,NH_4NO_3, reacts when fuel is added to it, producing gas and heat and increasing the temperature and power of a given explosion [12]. ANFO is a non-ideal low-density explosive, with a low detonation velocity (3 - 5 km/s) [19]. ANFO is one of the most widely used explosives in the mining industry and civil construction [20]. It is also commonly used as the main explosive in IEDs [18].

Figure 1.4: Ammonium Nitrate Fuel Oil prills. [12]

1.2 Characterization and Scaling of Explosives

Researchers in the past have investigated several visualization techniques that allow for observing and analyzing density and pressure gradients. The information obtained using this techniques has also been complimented with TNT equivalences. Schlieren photograph and shadowgrams have been used by Kleine et al., to analyze charges of varying masses of silver azide (AgN_3), a chemical compound which is used as a primer or primary explosive [4]. Kleine et al., compared the shock wave radius vs time profiles created by the detonation of AgN_3 to those that would have been produced by detonations of samples of the same mass of TNT [4]. This was done to find the TNT equivalences of silver azide at different ranges of mass. Kleine et al. used the resulting shock wave radius versus time profiles to determine the shock Mach number and hydrostatic overpressure, both as a function of the shock wave radius [4].

More recently, Biss et al. [6] used high-speed digital shadowgraph visualization at a laboratory-scale to track the shock wave radius versus time profiles of several composite explosive charges. Using this technique, the removal of the main effects of the composite charges booster component was achieved and the air-blast properties were obtained. Such blast properties were later used to

characterize the candidate explosive material. The resulting characterization of each composite was then used to find the TNT equivalence corresponding to each composite explosive charge [6].

The characterization of an explosive material is made possible by observing its physical properties [6]. In a simple form, the characterization of an explosive is the quantification of its blast parameters relative to a standard [21]. In order to calculate the relative energy released by an explosive, the radius of the shock wave needs to be determined and the physical property identified. Such value is typically related to the distance at which the same property occurs after a TNT detonation of the same mass is set off (i.e. TNT equivalence) [4][6][9][21][22]. However, this comparison can quickly become expensive and sometimes impractical at a large scale, because a description of the differences in shock wave motion when different explosives are used cannot be achieved. In order to better characterize an explosion, the radius vs time profiles and the overpressure duration profiles should be provided, not just the TNT equivalence [22].

Explosives are most commonly scaled using the Hopkinson or Sachs scaling laws [7] [22] [23]. Hopkinson showed that if a peak property value of a charge with mass W_1, or energy release E_1, occurs at distance R_1, and at distance R_2 from another charge of mass W_2 (or energy E_2) and the same material then:

$$\frac{R_1}{R_2} = \left(\frac{W_1}{W_2}\right)^{\frac{1}{3}} = \left(\frac{E_1}{E_2}\right)^{\frac{1}{3}} \tag{1.1}$$

Thus, the distance of the peak value of a specific property from the center of an explosive charge, and its duration, are proportional to the linear dimension of the spherical charge. The linear dimension of the charge is proportional to the cube root of the mass of the charge, ${W_1}^{1/3}$, and the cube root of the energy released, ${E_1}^{1/3}$ [23].

In 1944, Sachs investigated the atmospheric conditions of an explosives blast, assuming that a change in the scale of pressure, distance and time was due to the change in the external conditions [24]. Thus, Sachs added to Hopkinsons theory so it would account for temperature and pressure differences in the medium the shock wave traveled through [23]. Sachs scaling law relates explosions of varying masses in different atmospheres [21]. If the detonation in atmosphere of two materials of equal composition and different pressures is assumed, the scaled distance according to Sachs would be:

$$\frac{R_1}{R_2} = \left(\frac{W_1}{W_2}\right)^{\frac{1}{3}} \left(\frac{P_2}{P_1}\right)^{\frac{1}{3}} = \left(\frac{E_1}{E_2}\right)^{\frac{1}{3}} \left(\frac{P_2}{P_1}\right)^{\frac{1}{3}} \tag{1.2}$$

where R, W, P, and E denote the distance, weight, pressure, and energy, respectively, and the numbers 1 and 2 refer to the material in question. For this thesis, the results are scaled to a 1 kg charge (W_{STP}) at Normal Temperature and Pressure (T_{NTP} = 288.16K, P_{NTP} = 101325 Pa), as done by Hargather [11]. Thus, Equation 1.2 reduces to

$$\frac{R_1}{R_2} = \left(\frac{W_1}{W_{\text{STD}}}\right)^{\frac{1}{3}} \left(\frac{P_{\text{NTP}}}{P_1}\right)^{\frac{1}{3}} \tag{1.3}$$

To scale time, t, the equation used by Sachs is:

$$\frac{t_1}{t_2} = \left(\frac{W_1}{W_2}\right)^{\frac{1}{3}} \left(\frac{P_2}{P_1}\right)^{\frac{1}{3}} \left(\frac{T_1}{T_2}\right)^{\frac{1}{2}} = \left(\frac{E_1}{E_2}\right)^{\frac{1}{3}} \left(\frac{P_2}{P_1}\right)^{\frac{1}{3}} \left(\frac{T_1}{T_2}\right)^{\frac{1}{2}} \tag{1.4}$$

which reduces to:

$$\frac{t_1}{t_2} = \left(\frac{W_1}{W_{\text{STD}}}\right)^{\frac{1}{3}} \left(\frac{P_{\text{NTP}}}{P_1}\right)^{\frac{1}{3}} \left(\frac{T_1}{T_{\text{NTP}}}\right)^{\frac{1}{2}} \tag{1.5}$$

Kleine et al. [4], and Hargather et al. [22], used different terms of the Sachs' scaling method, which is the approach used in the present work. Charges of C-4 and ANFO, both encased and uncased, were scaled to a 1 kg charge at normal temperature and pressure (NTP) values using the following equations:

$$R_s = \frac{R}{S}, \text{ and } t_s = \frac{ct}{S} \tag{1.6}$$

where R_s and t_s represent the scaled values of the radius and time respectively, R and t represent the measured values of radius and time, while c and S are scaling factors given by:

$$c = \frac{T}{288.16K}^{\frac{1}{2}} \tag{1.7}$$

and

$$S = \left(\frac{W}{W_{STD}}^{\frac{1}{3}}\right) \left(\frac{101.325kPa}{P}\right)^{\frac{1}{3}} \tag{1.8}$$

Here, T and P are the ambient temperature and pressure measured in Kelvin and kPa, respectively, W is the charge mass in kg, and W_{STD} is the total mass which the charges are being scaled to, which in this case is W_{STD} = 1 kg.

After the results are scaled, the data points obtained from shock tracking are used and fit into a non-linear least squares equation (Equation 1.9) proposed by Dewey [25][4][11][22].

$$R_s = A + Ba_0t_s + Cln\left(1 + a_0t_s\right) + D\sqrt{ln\left(1 + a_0t_s\right)} \tag{1.9}$$

Here, A, B, C, and D are fitted coefficients, while a_0 represents the speed of sound at NTP. Coefficient B is set to equal 1 to ensure that the shock speed approaches the ambient speed of sound as time reaches infinity, and hence satisfy the physical limitations on time [4][22].

In order to validate the outcome of the scaling process used in this work, the scaled results of the C-4 experiments presented on this thesis are compared to the results obtained using the fitted coefficient values A, B, C, and D given by Equation 1.9 by Hargather [11].

1.3 Background - Oriented Schlieren

Although the visualization methods discussed above have been proved to be effective in small scale analysis, trying to adapt these systems to a large scale analysis can be difficult due to the size of the optical components required. The background oriented schlieren (BOS) technique is a method that can easily be adapted to both small and large-scale experimentation, because it does not need any precision optical components, thus it is an excellent choice when performing analysis at a large scale outdoors [8][9][10][11].

The BOS technique was first explored by Dalziel et al. [26], and patented by Meier [27] in the same time period [11]. The BOS technique requires a camera focused on an undisturbed background, against which light distortions are imaged [28]. Figure 1.5 shows a common optical arrangement for the background oriented schlieren technique. In a laboratory environment, the background is commonly a black-and-white dotted pattern. In the test region, the schlieren object is placed and the light is refracted through angle ϵ at point P. This refraction causes a distortion, which is imaged as a shift in the background [10].

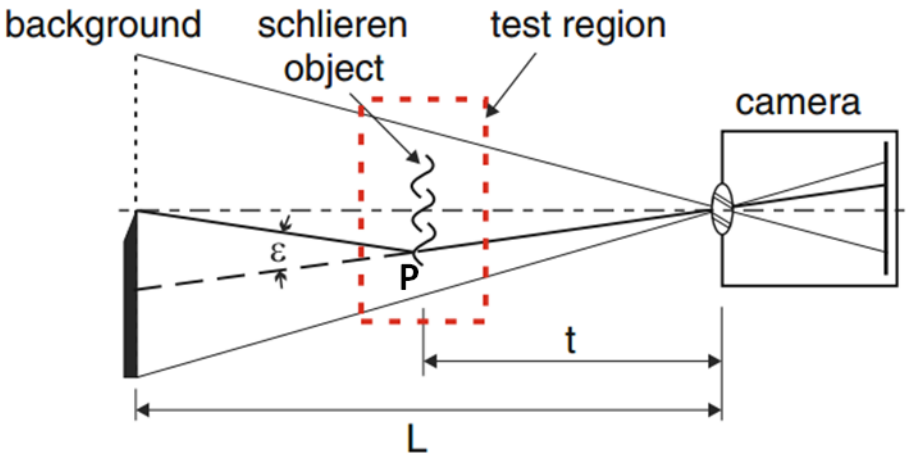

Figure 1.5: Typical Background Oriented Schlieren Set-Up

The light distortions are caused by refractive disturbances, which are regions in space with refractive index gradients [8]. For a gas, the refractive index is a function of the gas species and the gas density. Via the ideal gas law, this implies that temperature and pressure affect the refractive index of a gas. Because a shock wave generates density, temperature, and pressure gradients, the background oriented schlieren technique can be used to observe these gradients and thus, the shock wave.

Background Oriented Schlieren can be used to not only track the shock wave of explosives, but also to measure other density gradients. Klinge et al. proved that it is possible to use the BOS technique to determine the velocity and density distribution of a wing tip vortex created in the transonic wind tunnel of an aircraft [8]. Venkatakrishnan et al. used BOS to obtain the density field for a supersonic flow. The images obtained were processed using a cross-correlation algorithm, to obtain quantitative density measurements. The variations in density were then plotted against the location of the shock wave [29].

When the BOS process is used at a large scale, the setup shown in Figure 1.5 stays the same. However, because large-scale visualization experiments require a large field of view, the use of artificially generated random-dotted-pattern backgrounds is not practical [2][11]. In an outdoors environment, the use of artificial backgrounds is not required; instead, the use of natural backgrounds is possible [10]. This means that as long as there is something undisturbed behind the explosion, such as hills or trees, it will be likely to track the shock wave as far out from the origin as the camera frame permits.

Previous experimentalists have made use of pressure gages to track and obtain quantitative measurements of shock waves [30][31]. However, characterizing the energy release from large explosions using traditional point-pressure gages can quickly become difficult and expensive, and the set up for these experiments can be time consuming. The background oriented schlieren technique is used here to provide large-field-of-view visualization of the shock wave propagation from large-scale explosions. This technique is used to allow field measurements of blast wave properties instead of traditional point-wise measurements, since previous studies have shown that there had been discrepancies between pressure measurements obtained using pressure gages and BOS images [32]. Noise and especially fragments produced from an encased explosion can interfere with the readings, which leads to erroneous data being collected [33]. However, the measurements of the shock wave overpressures can be obtained using the BOS technique [9], which minimizes the error introduced due to noise and fragments, which can be ignored if the shock wave front is tracked directly.

The BOS technique can be used in situations where a high explosive is not detonated for experimental purposes. In real life scenarios, it is more likely to have a camera recording an event than pressure gages taking measurements at the right locations. Because the BOS method only requires a camera and a background, it can be applied everywhere where a camera is recording.

When high speed images undergo the BOS process, quantitative measurements of shock waves can be obtained. Sommersel et al., used this technique to

calculate the Mach number and predict the shock front overpressure of Composition C-4 high explosive [9]. The results obtained were compared to the C-4 mass equivalent of TNT at a given pressure, showing a good agreement between the experimental results and the theoretical results. The experiments performed by Sommersel et al., showed that the BOS technique is effectively used to estimate explosion overpressures from high explosives at a large scale.

Composition C-4 is a high explosive that has been commonly used alongside with the BOS technique [9][11][31]. The BOS technique was recently applied to a large-scale analysis of the detonation of Composition C-4 [11]. The shock propagation Mach number of C-4 was obtained from these experiments by using the BOS technique and a hill side as the natural background for the high-speed images. Hargather also used the optically-measured Mach numbers to estimate the reflected pressure and overpressure duration obtained at different pressure gage locations [11].

Another attempt to visualize the shock wave propagation of an open-air explosion of Composition C-4 was performed by Mizukaki et al. [31]. In this experiment, a high speed camera at a frame rate of 10,000 Hz, and 800 x 600 pixels field of view, was utilized. Mizukaki et al. also used a natural background that included trees and grass to make the measurements, instead of a random dot pattern commonly used in laboratory scale experiments. From the recorded images, Mizukaki et al. was able to obtain the shock wave propagation curve and overpressure distribution of C-4. The results were then compared to those obtained in a numerical analysis. There was a good agreement between the experimental and numerical results, which suggested that using the BOS method in an open field set up could provide better quantitative visualization results [31].

Following the examples described above, this thesis work focuses on using the BOS technique to obtain quantitative measurements of shock wave propagations of two main high explosives, Ammonium Nitrate Fuel Oil, and Composition C-4. From the shock wave propagation measurements, the Mach number as a function of radius can be obtained [11], and from these results, the overpressures can be predicted [9][11][31].

CHAPTER 2

EXPERIMENTAL METHODS

All experiments presented were performed at the Energetic Materials Research and Testing Center (EMRTC), which is a major research and training division of New Mexico Tech, and is located in Socorro, New Mexico. EMRTC specializes in the research, development, testing, and analysis of energetic materials. The facilities at EMRTC include more than 30 test sites, gun ranges, and other research facilities and storage areas, having the ability to perform tests using up to 50,000 pounds of explosives.

2.1 High Speed Video Equipment

The main camera used for this experiment was a Phantom v711 camera, manufactured by Vision research [34] and shown in Figure 2.1. This camera has an internal memory of 8GB RAM. The maximum resolution possible with the Phantom 711 is 1280 x 800, with a recording speed of 7530 frames per second (FPS). This camera is also capable of recording images at a maximum speed of 1,400,00 FPS when using the reduced resolution of 128 by 8 pixels [34]. The Phantom v711 uses the Phantom PCC 2.14b software to view and edit the recorded high speed videos. This gray-scale camera was used based on its recording capabilities and availability to document all pipe bombs, car bombs, and bare charges.

Figure 2.1: Phantom v711 digital high-speed camera by Vision Research. [34]

A digital Nikon D5100 digital camera was used to take photographic images of the tests final set-up, and the field before and after the explosions. A Nikon ED Nikkor 80 - 200 mm lens, and a Nikon DX AF-S Nikkor 18 - 55 mm lens were used for the high speed camera and the digital camera respectively.

Due to the intensity of the explosions and the needed location of the high speed camera, an aluminum box, shown in Figure 2.2, was built to protect the camera and its components. Plexiglas was placed in front of the camera lens to prevent fragments from hitting the lens or any other camera parts.

Figure 2.2: Aluminum Box of 0.25" thick plates protecting the Phantom v711 high-speed camera.

The high speed videos are recorded at a specific frame rate, which depends on each particular setup and environmental conditions. Once the video of the detonation is recorded, the video is converted into images. These images are then analyzed in MATLAB, where the BOS processing is performed. The BOS technique identifies pixel shifts in an image relative to a reference image. The pixel shifts are due to refractive disturbances that are present between the background and the camera and that change as a function of time. The shock wave that is produced from a car bomb or a pipe bomb explosion is a strong refractive disturbance with large density and pressure gradients across it. In these experiments, the shock wave is visualized with the BOS technique in each of the high-speed images. The BOS-processed images are then used to calculate the shock wave propagation velocity, and Mach number, among other characteristics of the explosion.

For a typical schematics of the BOS technique like the one shown in Figure 1.5, the smallest density gradient detected is what commonly determines the sensitivity of the system, which is a function of the capabilities of the camera, the strength of the object being analyzed, and optical geometry [10]. The sensitivity of the BOS process is also influenced by the L-t distance, shown in Figure 1.5, which is the distance between the object being analyzed and the camera, t, and the distance between the camera and the background, L. When the distance between the camera and the background, the focal length of the lens, and the resolution of the camera, are greater, the sensibility of the system improves, although it is important to maintain the background and the schlieren object in focus [10]. If the background is not focused, the shift in pixels is practically impossible to detect, even with the best resolution, and if the schlieren object is not focused, the images obtained are not of use. Thus, keeping a balanced focus is imperative for this process to function to its full capabilities.

2.2 Experimental Setup for C-4 Bare Charges and Pipe Bombs

The detonation of a total of six charges containing different masses of Composition C-4 was performed at the West Valley test range at EMRTC. These charges were detonated in the form of three Schedule 40 galvanized pipe bombs with dimensions shown in Figure 2.3, and three bare C-4 charges (Figure 1.3), requiring a total of 850 grams of C-4.

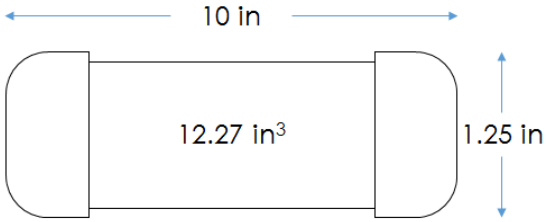

Figure 2.3: Schematics of galvanized pipes used for C-4 pipe bombs

The experimental setup for both bare C-4 and the encased charges was the same, and it is shown in Figure 2.4. The charges were placed on the ground with a sandbag underneath them. The high speed camera was placed perpendicular to the charges, where the horizontal center of the pipe bomb was in the center of the field of view of the camera. This was done to prevent the pipe caps from hitting the camera during detonation. The camera was placed inside an aluminum box to prevent fragment damage, which allowed for the camera to be placed at ground level approximately 41 meters from the charges (Figure 2.5).

All the pipes used for this experiment had the same dimensions, shown in Figure 2.3. EMRTC provided all the C-4 needed for the test. Using the properties of C-4 provided by EMRTC, shown in Table 2.1, the maximum amount of C-4

Figure 2.4: Aerial view of schematics for the pipe bomb and bare C-4 shots

that could be held by the geometry of the pipes is 315 grams. Thus, the upper limit of the test was set up at 300 grams.

The range of mass of C-4 in the different charges, shown in Table 2.2, al-

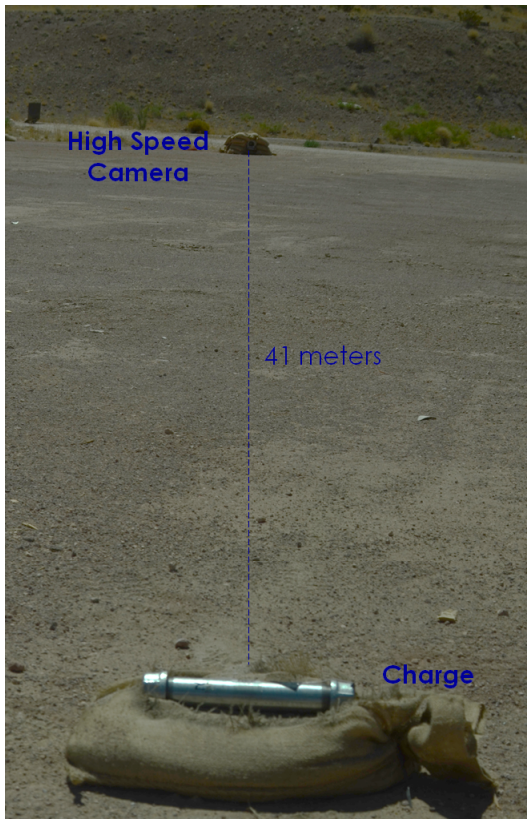

Figure 2.5: Physical view of experimental set up

Table 2.1: Composition C-4 Properties

Composition	91% RDX - 9% Polyisobutylene
Density (g/cm^3)	1.60
Density (lb/ft^3)	99.88
VoD (m/s)	8092

lowed for the determination of the scalability and repeatability of C-4. The C-4 inside the pipes was placed as close to the center as possible to minimize symmetry errors. The high speed videos of these shots were recorded and processed via the BOS technique. Then, shock wave radius vs time profiles, and the Mach number vs shock radius profiles were obtained.

Table 2.2: Test Matrix of C-4 Pipe Bombs and Bare Charges

Charge Number	C-4 Mass (g)	Type of Charge	Distribution of Explosive
1	50	Bare Charge	Center of test area
2, 3	50	Pipe Bomb	Center of pipe bomb
4	100	Pipe Bomb	Center of pipe bomb
5, 6	300	Bare Charge	Center of test area

The setup of the test required running trigger, ethernet and power lines from the bunker, on the right side of Figure 2.4, to the camera. While the test took place, the camera was armed and monitored from inside the bunker. The camera activated at the same time the explosives were set off using a RP-83 explosive bridge wire initiation system. The firing details are shown in Figure 2.6.

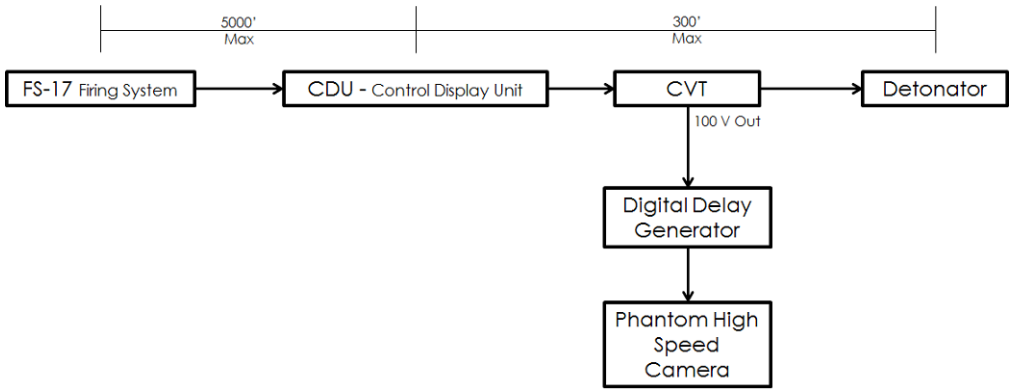

Figure 2.6: Firing details for the initiation of explosives and triggering of high speed camera

The FS-17 EBW (explosive bridge wire) was the firing system used here because the explosive charges and the high speed cameras were activated at the same time. Thus the module voltage needed to be monitored. The maximum

distance allowed between the FS-17 and the CDU is 5000 feet. The control unit (CDU), which kept the communication between input and output devices, can only be 300 feet from the detonator. The CDU send the signal to a CVT, which then activates the detonator. A delay generator by Stanford Research Systems regulates the delay needed for triggering the detonators and the Phantom camera. The Phantom camera is set to rising edge, which allows the camera to activate when there is a rise in voltage. Environmental parameters were noted hourly for scaling purposes.

After the field of view for each test was determined, calibration measurements were made to be able to convert pixel distances viewed in the high speed images to true distance values in meters. To accomplish this conversion, an object of known length was placed in the field of view, and an image was taken with the high speed camera. Then, the length of the object in pixels was divided to its length in meters, resulting in a pixel per meter ratio, which was used when calculating the diameter of the shock wave. When recording the high speed videos of the bare charges and pipe bombs, a variation of resolutions and speeds were used. These variations are shown in Table 2.3. Because the camera was always looking at the same area and was never moved, the calibration measurements were not influenced by the resolution or the frames per second at which the high speed videos were recorded.

Table 2.3: High Speed Camera Parameters Used Per C-4 Shot

Charge Number	Resolution	Speed (FPS)
1	1024 x 800	8000
2	1024 x 800	8000
3	1024 x 800	8000
4	1024 x 800	8000
5	256 x 800	25000
6	1024 x 800	9000

Once the videos were recorded, they were taken to the laboratory where they were processed using MATLAB.

2.3 Experimental Setup for Encased and Uncased ANFO

Several charges of encased and uncased Ammonium Nitrate Fuel Oil (ANFO) were detonated. These detonations took the form of car bombs and one bare charge, and were recorded using a Phantom v711 high speed camera (Figure 2.1). The purpose of these experiments was to characterize ANFO to gain a better understanding of its physical properties, and investigate its scalability potential. The car bombs recorded formed part of a demonstration EMRTC performed as part of the First Responder Training Program.

A total of 4 car bombs were recorded and analyzed. The experimental set-up for the car bomb detonations (Figure 2.7) did not vary between shots. The distance between the high speed camera and the car was 210 meters. Although this distance is far from the center of the charge, the camera was placed inside an aluminum box to prevent any fragment damage. The explosive charge remained the same for all shots and was placed in the truck of each car. The casing, or vehicle detonated, varied in dimensions and style, specified in Table 2.4. Each car had its air bags removed, and the gas tank emptied for safety purposes.

Figure 2.7: Areal view of the experimental set up used for car bombs containing ANFO

Table 2.4: Test Matrix for Car Bombs Containing ANFO

Charge Number	ANFO Mass (kg)	Type of Car	Temperature (° F)	Pressure (Pa)
1	113.4	1999 Ford Escort	86.7	101625
2	113.4	1990 Toyota Cressida	81.0	101287
3	113.4	1996 Saturn SL	77.9	102032
4	113.4	1994 VW Caddy Pick-Up	64.8	101659
5	1.59	Uncased Charge	67.8	101219

All car bombs were detonated between the hours of 1:30 pm and 3:15 pm on different days, and even though pressures and temperatures varied, clear skies were the overall weather condition. An additional bare shot of ANFO was recorded. The results obtained from this video were used to compare how casing affects the shock wave velocity and Mach number of ANFO. Both temperature and pressure for each shot can be found in Table 2.4.

Ethernet, power and trigger lines ran from the bunker to the camera. The camera was remotely monitored from the bunker. A hand trigger was used to

activate the camera, while the explosive charge was initiated separately using an FS-17.

Figure 2.8: General placement of charges inside the trunk of a car

The ammonium nitrate fuel oil used was that provided by EMRTC. For all shots, the explosive charges were placed in the trunk of each car (Figure 2.8). The charges were dual primed for safety and reliability of detonation. The dual priming did not affect the results of the explosion. The properties of the ANFO used are shown in Table 2.5

Table 2.5: 94% Ammonia Nitrate Prill / 6% Fuel Oil ANFO Properties

Bulk Density (g/cm^3)	0.84
VoD (m/s)	2400 - 4750

Similarly to the C-4 experiment, calibration measurements were performed. The calibration measurements were different for every car bomb because the field of view from one shot was not identical to the next. Table 2.6 indicates the parameters of each video taken.

Table 2.6: High Speed Camera Parameters Used Per ANFO Shot

Charge Number	Resolution	Speed (FPS)
1	512 x 608	18003
2	448 x 800	16000
3	512 x 800	8000
4	512 x 800	6000
5	800 x 800	5000

2.4 Background Oriented Schlieren Algorithm

After recording the high speed videos of the detonation of C-4 and ANFO, they were analyzed using the BOS technique (Figure 2.9). In order for this process to take place, the high speed videos were converted into high speed images. Using these processed high-speed images, the shock front was visualized using a computer algorithm.

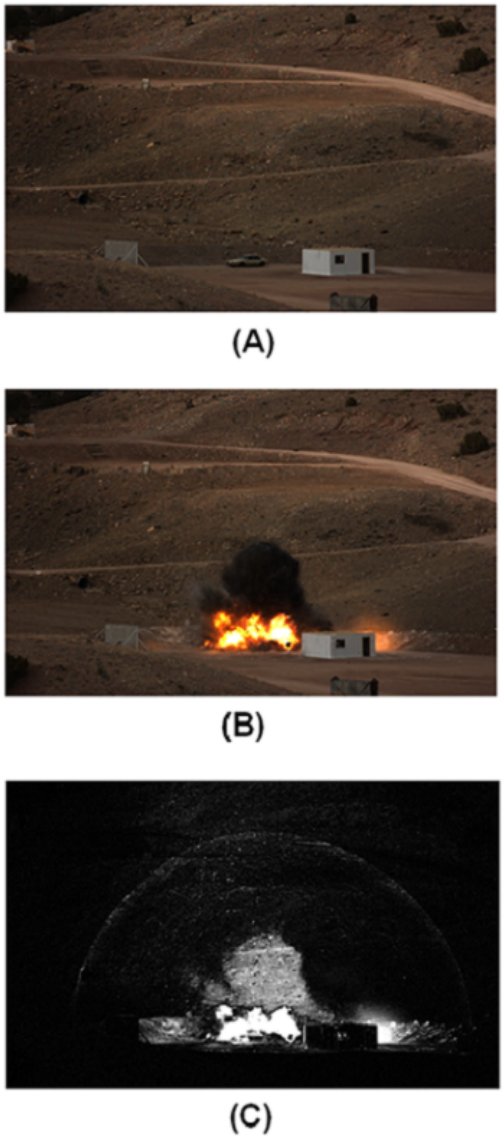

Figure 2.9: Background oriented schlieren image processing. The undisturbed image (A) is subtracted from a disturbed image (B), resulting in an image that shows the density and pressure gradients of the shock wave (C).

The BOS processing requires an image of the undisturbed background to be taken (Figure 2.9A). Due to the size of the field of view, the background used for all experiments was a hillside instead of a random-dotted pattern. The images obtained during the detonation of the car bomb contained density and pressure gradients (Figure 2.9B). The computer algorithm subtracts the undistorted image from those images with density and pressure gradients, resulting in a series of images with a highlighted, easy-to-track shock front (Figure 2.9C).

The displacement of the shock wave observed from one image to the next, shown in Figure 2.10, is used to calculate the shock wave position versus time profiles, and Mach number versus radius profiles. The application of the BOS technique to high-speed videos helps obtain quantitative measurements of shock waves of a particular explosion.

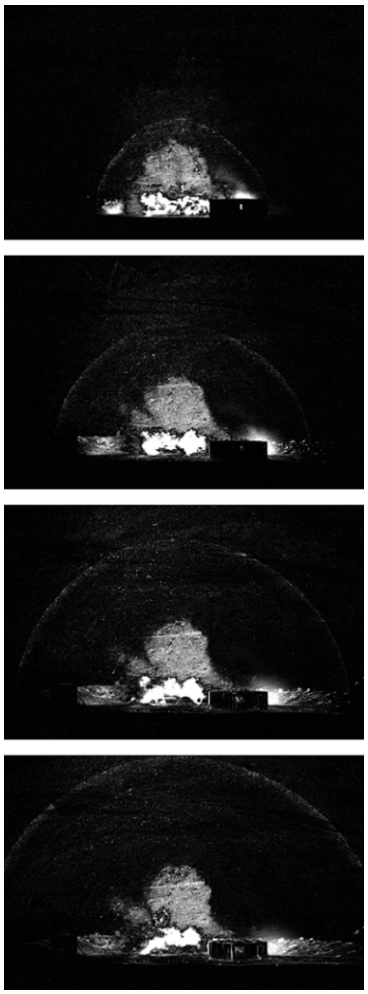

Figure 2.10: BOS images clearly show the expanding spherical shock wave from the car bomb explosion. Images are 12.2 milliseconds apart.

2.5 Computer Algorithm for Shock Wave Tracking

Once the gray-scale images are processed using the BOS technique, they are processed with another computer algorithm that measures the shock wave radius as a function of time [21]. This algorithm takes each image with a highlighted shock (Figure 2.10) and back-tracks the shock wave from the edge of the field of view to the center of the charge. Because the frames per second of each shot is known (Tables 2.3, and 2.6), the time at which each image was taken is also known. For this particular experiment, the code required the user to manually enter the center of the charge coordinates, and radius of the shock wave at each frame in pixel units.

The center of the explosion did not always match the center of the IEDs. In the case of the car bombs, the explosive was placed in the trunk of the car, which meant that the center of the explosion would be somewhere in the centerline of the trunk. For the pipe bombs, the center of explosion originated at the center of the IED for the most part. Nevertheless, there were a few occasions where the explosive was not placed exactly in the middle of the pipes. Thus, instead of using the center of the casing, the first frame where disturbances were observed was used to more accurately locate the center of explosion.

Figure 2.11: Using an undisturbed image, the length of the calibration object is measured in pixels, and compared to its equivalent in meters.

The algorithm uses the conversion factor to obtain the radius of the shock

wave in meters from the pixel measurement. This conversion factor is unique for every experiment, and it is obtained by measuring the distance in meters of an object perpendicular to the camera and located along the centerline of the object of interest, as shown in Figure 2.11. Other required input for the algorithm is the explosives mass, the ambient temperature and pressure of each shot, estimated unit conversion errors, as well as the frame rate at which the video was taken. With this inputs in place, the algorithm backtracks the shock wave, starting at the last image where the shock wave is present, and ending at the first image where no disturbances are present.

The algorithm makes radius measurements and fits them to Equation 1.9, and outputs the sequence image number, the location of the shock wave with respect to time, the Mach number at each image point, and the error on both the shock radius and the Mach number. Other outputs also include x-t diagrams, and a movie that shows the shock wave movement backwards in time. The aforementioned outputs help identify any human errors present in the shock wave tracking.

The velocity of the shock wave at each frame is calculated using a centered difference in radii over the difference in time. The velocity is then used to plot the Mach number at each radius point. The Mach number is used to identify the various physical properties of a shock.

CHAPTER 3

EXPERIMENTAL RESULTS AND DISCUSSION

Once the high speed videos of the detonation of C-4 and ANFO were processed using the algorithm described in Section 2.5, the output data were analyzed. The information gathered was used to generate shock wave radius versus time profiles for each test. From these data, the scaled radii and time were calculated and plotted. In addition, the shock wave Mach numbers were calculated and plotted with respect to scaled radii. The Mach numbers of each profile served to obtain pressure profiles with respect to scaled radii.

The data presented here does not represent all the tests that took place. Some pipe bombs were not included because the explosive material was not C-4, but rather smokeless powder. Several car bombs were recorded, but only the best results are presented. The excluded tests were not included because the data obtained from the videos had too much noise and/or fragments crossing the shock, which made it difficult to identify which pixels represented the shock front and which were just part of debris. Only the results of the processed high speed images with a clearly defined shock are presented.

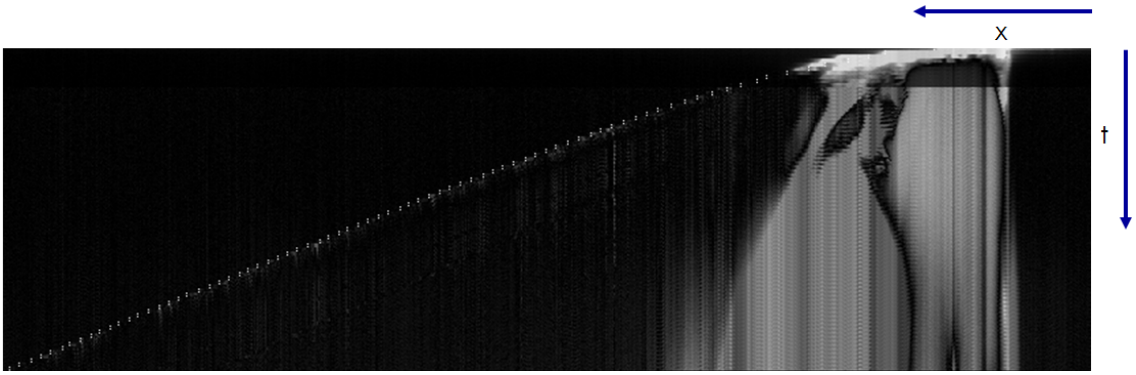

Figure 3.1: x-t diagrams for a 50-g bare C-4 charge obtained from the shock wave tracking algorithm.

To determine which data sets would be used, the streak images obtained from the BOS process were taken into consideration. As mentioned in Section 2.5, the computer algorithm outputs position versus time (x-t) diagrams. These diagrams are a simple way to check if the algorithm is correctly tracking the shock

wave. These x-t diagrams highlight the shock with a single line of pixels as time increases, as detected by the computer program. The streak diagram in Figure 3.1 shows the program is detecting the right location of the shock wave, and thus, this set of data can be used for further analysis.

3.1 Shock Wave Location versus Time Profiles

The shock wave radius versus time profiles of all pipe bombs, bare C-4, car bombs and bare ANFO charge were obtained from the information outputted by the computer algorithm.

3.1.1 Composition C-4 Bare Charges and Pipe Bombs

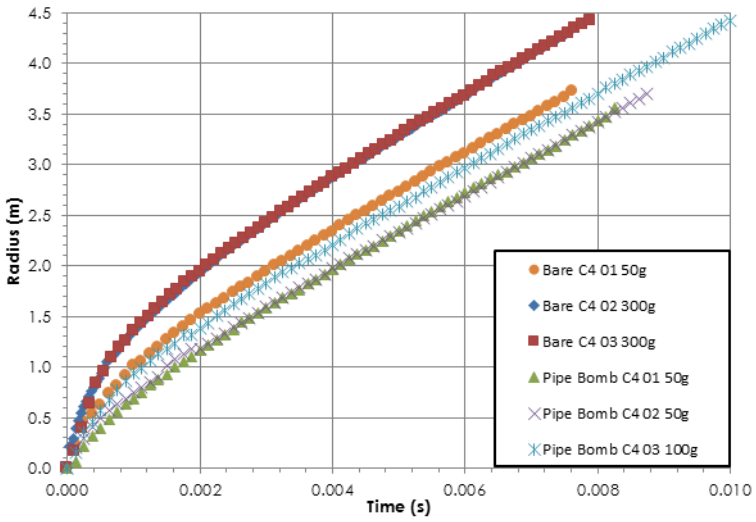

Figure 3.2: Un-scaled Shock Wave Radius vs Time profiles for bare C-4 charges and pipe bombs at different masses.

The profiles of confined charges of the same mass, and bare charges of the same mass, overlap as expected, as shown in Figure 3.2. The shock wave created by the bare charge of 50 grams of C-4 is propagating slightly faster than the shock wave of the pipe bomb containing 100 grams. This is due to the fact that the fragments of the galvanized pipe absorb energy from the expanding gases and reduce the shock wave propagation speed [23]. The error in these profiles is smaller than the size of the markers, and the uncertainty of the radii measurements is $\pm$ 0.01 m. The general trend of the profiles presented here indicates that the shock wave starts traveling at a high speed, and then it decays. Thus, even though the radius of the shock wave is increasing, it is not doing so at a constant rate.

In order to be able to make a comparison between each profile obtained, the resulting shock wave radius vs time profiles are scaled to 1-kilogram charges of C-4, shown in Figure 3.3.

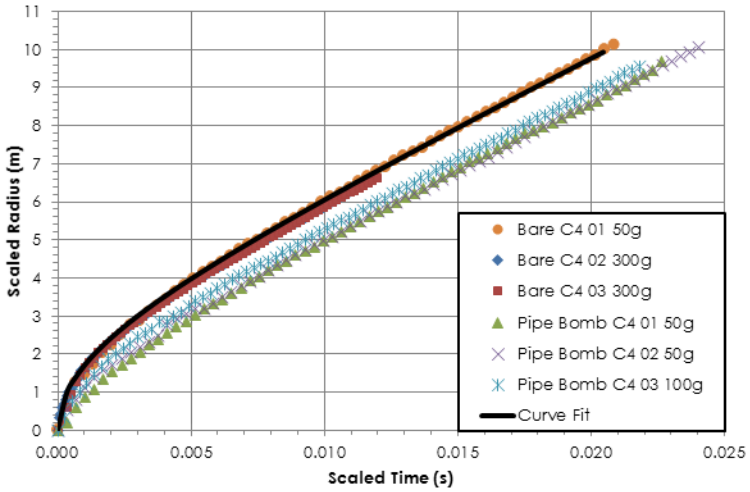

Figure 3.3: Scaled Shock wave radius vs Time profiles for bare C-4 charges and pipe bombs at different masses.

The scaling laws used were the Sachs laws, which were previously described in section 1.2. For each profile, the scaling factors c and S (Equations 1.7 and 1.8) were unique. These scaling factors were obtained by using the ambient temperatures and pressures measured at the same time each shot took place, as well as the mass of charge detonated. All profiles were scaled to a 1-kilogram explosive charge, hence the value of W_{STD} stayed constant. For every high-speed video analyzed, the measured radii at each frame, the time of each frame, and its corresponding scaling factors were used in Equation 1.6 to calculate the values of scaled radius and scaled times.

It is observed in Figure 3.3 that the profiles for uncased C-4 overlap with each other, as is the case of the cased C-4 profiles, regardless of the weight of explosive used per shot. The uncased and encased scaled profiles do not overlap because there is energy lost due to fragmentation of the pipes containing the explosives. However, regardless of the casing, these profiles become close together. The coefficients shown in Table 3.1, along with Equation 1.9, were utilized to obtain a curve fit for the bare charge profiles, which is plotted along with the Composition C-4 scaled results.

Table 3.1: Experimental and reported curve fit coefficients for Bare C4

Coefficients	A	B	C	D
Experimental	-0.14568	1.0000	-0.25226	2.5488
By Hargather	0.010656	1.0000	-0.48533	2.7577

This curve fit is plotted in Figure 3.4, along with a curve fit obtained using the coefficients reported by Hargather [11]. As it can be seen, the curve fit profile of uncased C-4 agrees with the profile obtained using Hargathers coefficients. The small discrepancies observed between these curve-fit profiles is attributed to the difference in experimental set-ups, and uncertainties present in the measurements.

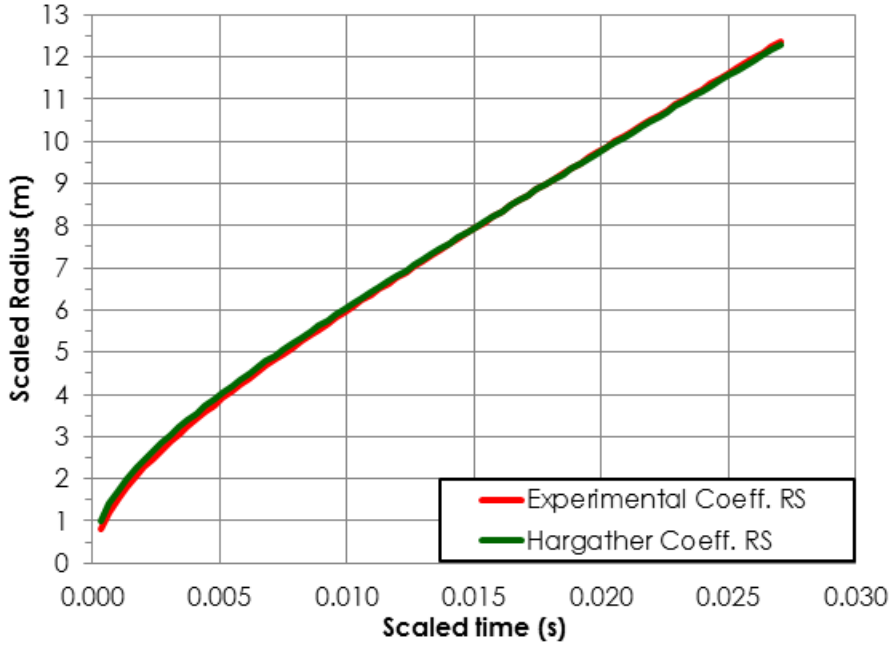

Figure 3.4: Curve fit profiles for bare C-4 obtained using coefficients in Table 3.1.

Coefficients for the scaled pipe bomb profiles were also calculated (Table 3.2), and used along with Equation 1.9 to obtain a trend line for encased C-4. A comparison between the curve fits of bare C-4 charges and C-4 pipe bombs can be observed in Figure 3.5. To obtain a mass difference between these two profiles, the curve fit of bare C-4 was forced to overlap with the curve fit of encased C-4 by changing the value of S (Equation 1.8). This resulted in a mass value of μ of 0.16 kg, which indicates that a 0.16-kg charge of bare C-4 would have the same shock wave characteristics as a 1-kg C-4 pipe bomb.

Table 3.2: Experimentally Obtained Curve Fit Coefficients for Encased C-4

A	B	C	D
-.013755	1.0000	-0.14898	1.4914

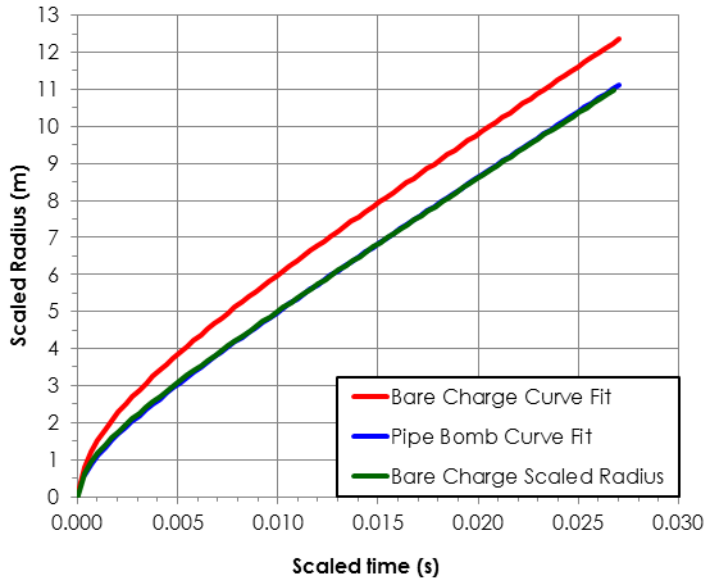

Figure 3.5: Least squared trend lines for bare and encased C-4.

3.1.2 ANFO Bare Charges and Car Bombs

As it was the case for C-4, the ANFO profiles also indicate a decay in shock propagation as the shock wave gets further away from the origin. The bare ANFO charge (Figure 3.6) shows a smooth, non-linear profile as expected. The shock

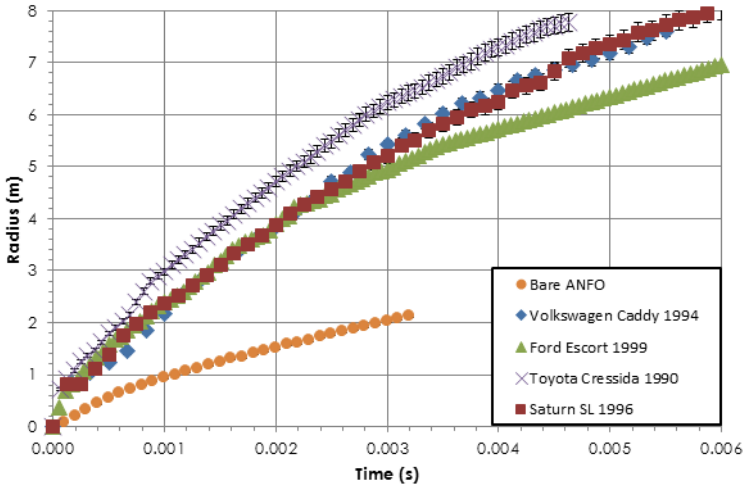

Figure 3.6: Un-scaled Shock Wave Radius vs Time profiles for bare and encased ANFO in the form of car bombs. Mass of ANFO bare charge = 1.6 kg. Mass of ANFO in car bombs = 113.4 kg.

wave is decaying as it propagates with time, but not at a constant rate. The shock created by this bare explosion did not require breaking any casing, and thus, the propagation of the shock wave is smooth. The error bars not shown are smaller than the size of the markers for each profile, and the uncertainty if the radii measurements is $\pm$ 0.06 m.

The profiles of the experiments performed with ANFO do not overlap, even though the same mass of explosive was used throughout, with the exception of the bare charge. Unlike the C-4 detonations, the ANFO experiments did not have a consistent casing. Every car used was a different style, make, and model; the materials the car was made out of were not the same, and the overall curb weight of the cars also varied. Moreover, the size of the trunks, which is where the explosive was placed, were different. Nevertheless, the car bomb profiles seem to have followed the same trend.

For comparison purposes, the ANFO profiles were scaled to a 1-kg charge as done for C-4. The profiles shown in Figure 3.7 reveals that the scaled values calculated for ANFO do not produce similar or overlapping profiles. This fact might be due to the inconsistency between experiments. Even when the fields of view, ambient temperatures and pressures, and amount of explosives were very similar in between shots, the results show that there are other variables that affect the repeatability of the results. In this case, the biggest difference between experiments was the material and size of casing.

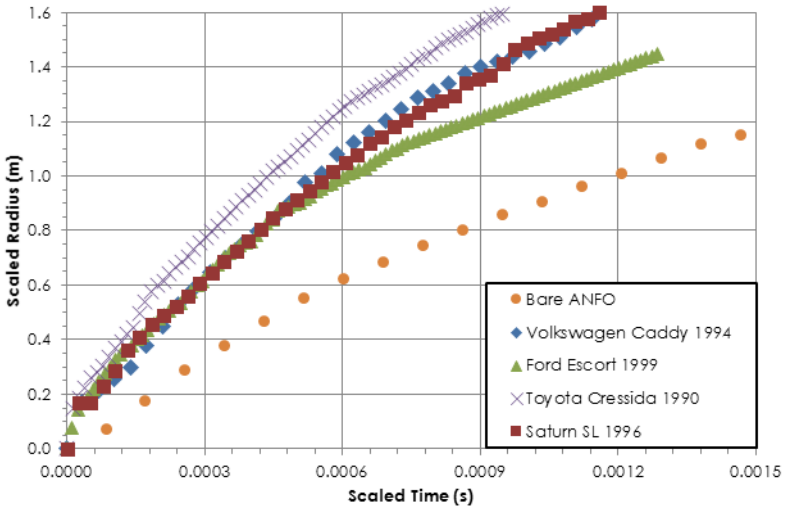

Figure 3.7: Scaled Shock wave radius vs Time profiles for bare ANFO charges and car bombs.

The profiles for the car bombs are not as smooth as the profile for the bare ANFO charge. This is attributed to human error and the inability to accurately detect the pixel indicating the leading edge of the shock wave. Unlike the bare C-4 charges, bare ANFO had to be placed inside a sono-tube because the prills of ANFO scattered when placing them directly on the ground. Thus, even the

bare ANFO charge lost some energy to destroying the casing. Moreover, the velocity at which ANFO detonates is influenced by the confinement of the charge; the better the confinement, the faster ANFO detonates. Because the total mass of the ANFO charges was confined inside the trunk of the cars (as opposed to distributed throughout the whole interior of the cars), a higher detonation velocity was achieved.

The mass of the ANFO charges remained constant between shots, which means the ambient pressures and temperatures were the only parameters influencing the scaling laws. The variations among these temperatures and pressures were very slight, and thus the scaled profiles get closer together, but do not overlap. Thus, even though the Sachs method takes into account atmospheric variations in pressure and temperature, the biggest influence of this analysis is the mass of the explosive charges. Moreover, because the encasing of the ANFO charges is not constant in dimensions, material or weight, as is the encasing of C-4, the energy lost due to fragmentation is different for each shot, affecting the consistency of the profiles and preventing them from overlapping.

The comparison between Figures 3.7 and 3.3 show that for an ideal explosive (C-4), the shock wave propagates faster when the explosive is not encased. The opposite is observed for non-ideal explosives (ANFO); the shock wave created by encased ANFO propagates faster than that of uncased ANFO. If smoother, and more uniform scaled shock wave radius versus scaled time profiles could be generated for ANFO, a scaling factor between bare and encased ANFO charges could be obtained, as done for C-4. However, because the results observed for ANFO were obtained from experiments with inconsistencies, such as the casing of the charge, the scaling factor for ANFO is not included in the present work. Nonetheless, based on Figure 3.3, it is predicted that a larger charge of bare ANFO would be needed to replicate the shock wave characteristics of a 1-kg charge of encased ANFO. Although a reason as to why this would happen has not been established, the results gathered in this work support previous observations that the detonation of encased non-ideal explosives creates a shock wave that is propagating faster than uncased non-deal explosives [35]. This is also shown by Catanach et. al., who performed rate stick tests on lightly confined ANFO at varying diameters, finding that ANFOs detonation velocity was deficient near the critical diameter [36].

3.2 Mach Number versus Shock Location

The Mach number is calculated using the centered finite difference from the radius profiles. Figures 3.8 and 3.9 show the distribution of the shock wave Mach number as a function of the scaled shock wave radius for the C-4 and ANFO charges respectively.

As it can be observed in Figure 3.8, the Mach number profiles followed the same trend, starting at high values, and then decaying to Mach 1 as the radius of the shock wave increased. The ANFO Mach profiles in Figure 3.9 show more

scattered data. However, the curve fit applied to these data indicates that the ANFO profiles follow a similar trend as the C-4 profiles, starting at high Mach values and eventually decaying to one. This curve fit was obtained by differentiating Equation 1.9 with respect to time. C-4 profiles are shown to be more uniform than ANFO profiles. This is because the detonation and properties of ANFO are not as ideal as those of C-4.

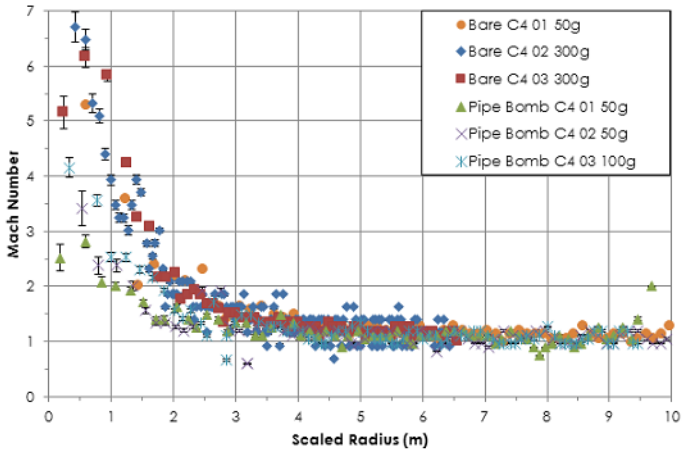

Figure 3.8: Mach number vs scaled shock wave radius profiles for all Composition C-4 charges.

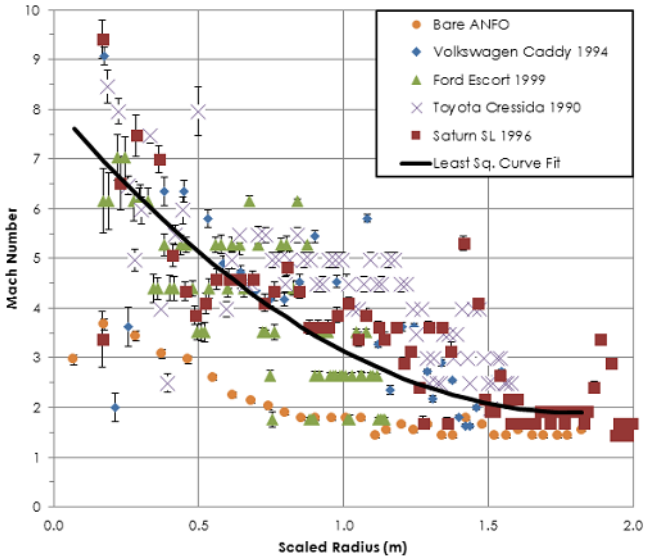

Figure 3.9: Mach number vs scaled shock wave radius profiles for all Ammonium Nitrate Fuel Oil car bombs and bare charges.

The scaled shock location as a function of time allows the derivation of

other important information specific to a given explosive, such as the Mach number versus shock wave radius profiles. Knowing the ratio of values of a physical property of a shock leads to the ability to calculate any other physical property of such shock. That is why if the Mach number, M, is known (Equation 3.1), other properties of the shock can be found, such as shock overpressures (Equation 3.2), gas densities (Equation 3.3), and absolute gas temperatures (Equation 3.4) [23]. Here, V_s is the velocity of shock wave, a_0 is the speed of sound through the medium, and γ is the ratio of specific heats of the gas.

$$M = \frac{V_s}{a_0} \tag{3.1}$$

$$P_2 = P_{ATM}\left(\frac{2\gamma\left(M^2-1\right)}{\gamma+1}\right) \tag{3.2}$$

$$\frac{\rho_2}{\rho_1} = \frac{(\gamma+1)\,M^2}{M^2\,(\gamma-1)+2} \tag{3.3}$$

$$\frac{T_2}{T_1} = \frac{\left(M^2 2\gamma-\gamma+1\right)\left(M^2(\gamma-1)+2\right)}{M^2(\gamma+1)^2} \tag{3.4}$$

3.3 Pressure Profiles

The shock wave Mach number can be related to the overpressure, P_2, via Equation 3.2. For Composition C-4, shown in Figure 3.10, it was found that the pressure rapidly increases during the first moments after detonation. As the radius of the shock wave increases, the overpressure of the shock decayed exponentially. These profiles are compared to computationally generated profiles in Chapter 4.

From these profiles, it was observed that the peak shock wave pressures for encased C-4 were much smaller than the peak pressures for uncased C-4. Also, the peak shock wave overpressure of uncased detonations was larger for larger mass charges. The cased charges profiles show the same behavior; pipe bombs with 100 grams of C-4 have a higher peak pressure than pipe bombs with 50 grams of C-4. The noticeable difference of peak pressure values between bare charges and encased charges is attributed to the fact that the casing absorbed energy to be broken apart.

For the ANFO experiments, plotted in Figure 3.11, pressure profiles are also gathered from the local Mach numbers. The peak overpressures for these profiles carry error with them. During the first few frames of the event, the fireball washed out the shock wave, making it difficult to get an accurate reading on the value of the shock wave diameter. Because the Mach number is calculated using this distance, the error was carried to the pressure profiles.

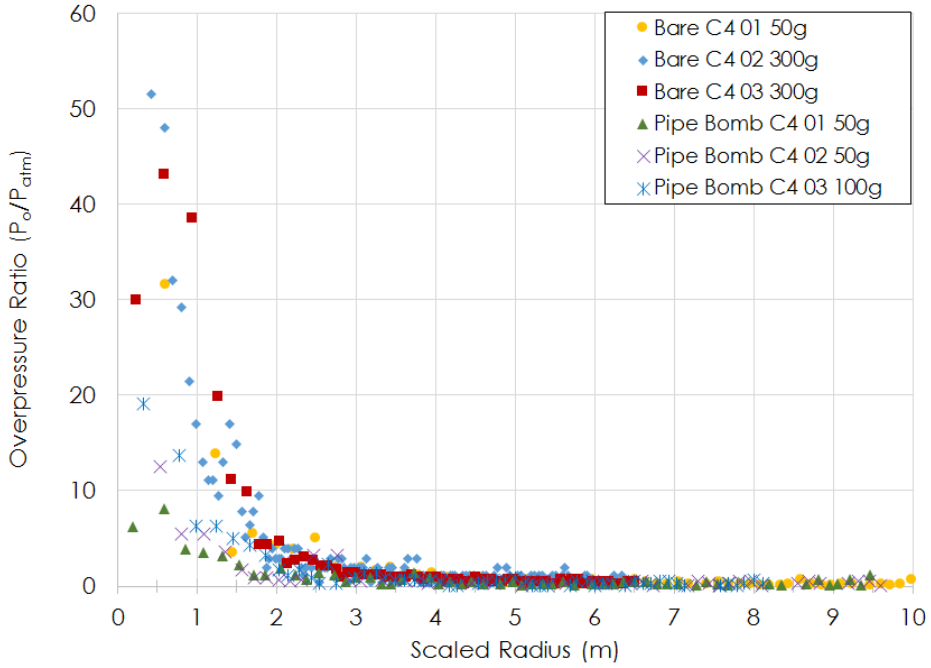

Figure 3.10: Overpressure vs logarithmic values of scaled radius for cased and uncased Composition C-4.

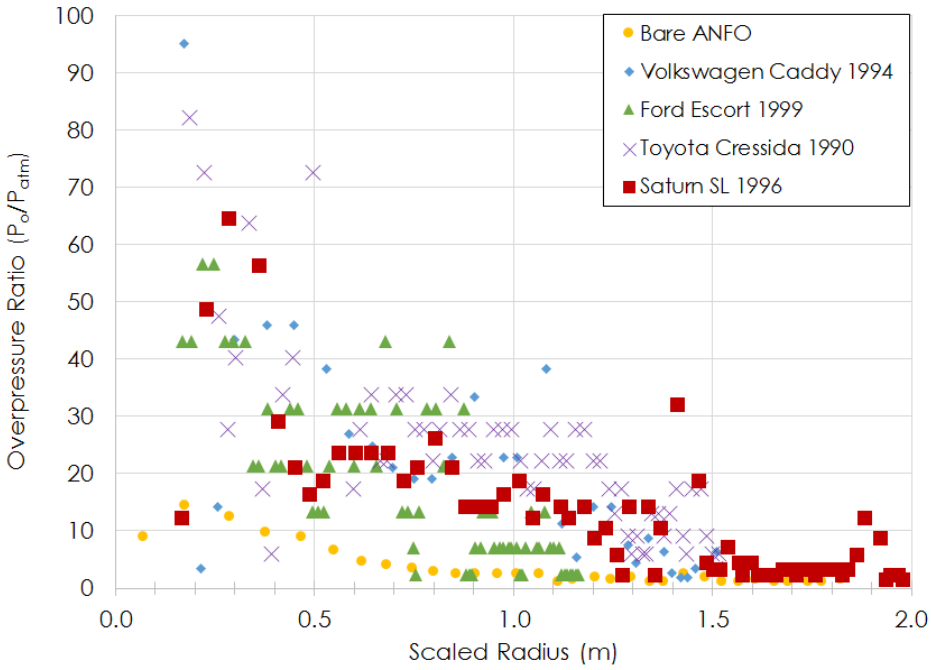

Figure 3.11: Overpressure vs scaled radius profile for cased and uncased ANFO.

3.4 Experimental Error

The measurements of radius as it approaches the center of detonation are another source of error. For the cased explosions, it is very hard to pin-point the center of the explosive or exact origin of detonation. The center of each detonation was determined to the best abilities by the user, introducing human error to the analysis. For the uncased explosions, it was easier to establish an origin for the explosion, with uncertainties of only ± 1 pixels. The detonation of the explosive charge released energy that was then absorbed by the casing, causing this to fragment in uncountable pieces. Some of these pieces passed the shock front, making it somewhat difficult to distinguish between shock wave and fragments. Thus, further human error was introduced when selecting the pixel that indicates the leading the shock wave, adding an uncertainty of ± 1 pixels.

The luminosity of the explosion conceals the visibility of the detonation products [23]. Although the fireball created by these explosions was not investigated, it is noted that it had an effect on the uncertainty introduced when tracking the shock wave approximately 1 meter away from the center of the car bomb detonations. To account for this error, it was assumed that the shock wave was spherical, and the visible shock on the sides was used to estimate the location of the shock wave perpendicular to the charge.

The exact time the explosives detonate is uncertain. The frame rate selected for each one of the high speed videos, however fast it was, did not record the instant the charges initiate. The charges detonated sometime between their respective frame zero and one, but the exact moment is unknown. Thus, time zero in the profiles is not exact, which means the profiles could be shifted along the horizontal axis approximately 0.001 second. For the analysis of these explosives, time zero was considered to be the time at the frame previous to the first frame with disturbances.

The high speed camera is capable of recording gray scale images. This made it difficult to identify the pixel representing the leading edge of the shock wave. Thus human error was brought out in the results. Calibration measurement errors were introduced the further the charge was from the camera. An object with known distance was placed in the field of view, but because it is far from the camera, and the camera is only capable of recording gray scale videos, the edges of the calibration object were not clearly defined. Nevertheless, the distance from the camera to both edges of the calibration object was measured repeatedly and averaged. These measurements helped determine the uncertainty in the calibration distances, which are ± 3 pixels for the ANFO charges, and ± 1 pixel for the C-4 charges. These uncertainties are specified and accounted for within the computational algorithm.

CHAPTER 4

CTH COMPUTER MODELING

Numerical simulations were performed using the hydrocode CTH. CTH is a computer modeling software developed by Sandia National Laboratories. This hydrocode allows for simulation of explosions. It is capable of simulating explosions in one dimension (rectilinear, cylindrical, and spherical meshes), two dimensions (rectangular and cylindrical meshes) or three dimensions (rectangular meshes). CTH uses second - order numerical methods, which reduce dispersion and dissipation to produce more accurate results [37].

The detonation of the explosives used for this thesis was modeled using CTH's Jones-Wilkins-Lee (JWL) formula. The medium was air modeled as an ideal gas. The results obtained using this hydrocode are compared to the experimental results. Only C-4 was simulated because an equation of state for ANFO was not available within the hydrocode.

4.1 Composition C-4 Computational Simulation

A 1-kilogram C-4 bare charge detonation was modeled using a 1-dimensional analysis and the JWL EOS. The charge is assumed to be spherical with a radius of 5.3 centimeters. This value was obtained using the density of C-4 (1.6 g/cm^2)and the mass of the charge (1kg). The center of the charge was considered to be at 0 cm. A tracer was programed to be every 5.3 centimeters, going out to 3.3 meters, giving a total of 63 tracers. Each of these tracers took pressure measurements as the shock wave passed through. The simulation outputs a spreadsheet with the number of tracers and pressures read over a period of $5E^{-3}$ seconds. CTH works with geometry regions called blocks, which have their own volume mesh, but share the same geometry among them. Here, it was determined that a ratio of 10 blocks per centimeter would be used. These blocks cover the total region being modeled, in this case, 500 centimeters. A temporal mesh is set according to the limits established by the user. The mesh lines are fixed, the quantities are cell centered, and the materials move through the mesh [38].

The output data were used to find the times at which the shock wave passed through each tracer. Because the distance between tracer is known, a shock wave radius vs time profile was created, and shown in Figure 4.1. The profile shows the expected trend: the radius of the shock wave increases as time

increases, but not linearly. The CTH simulation allows for an ideal scenario to be recreated.

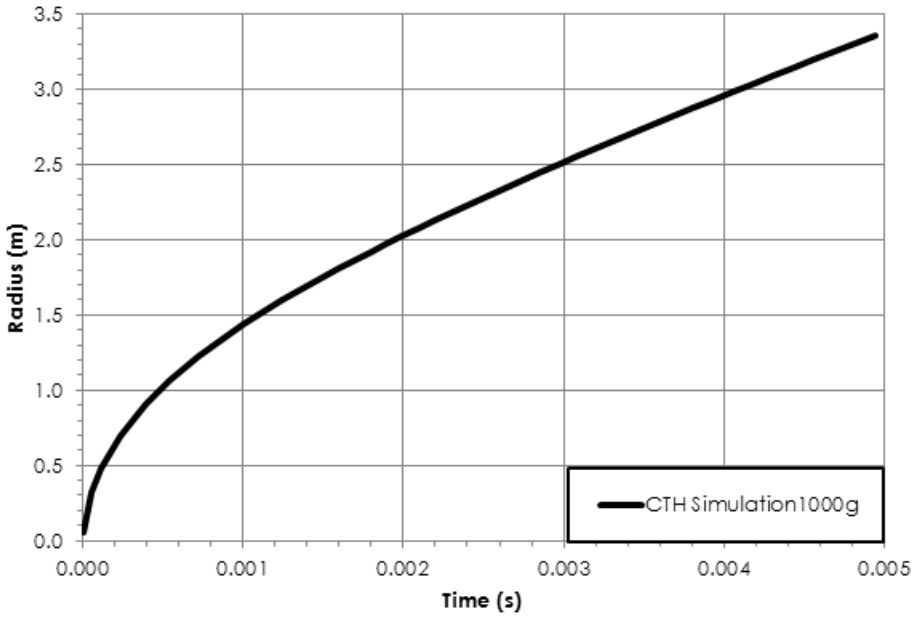

Figure 4.1: Shock wave radius vs Time profiles for a CTH simulation of a 1kg bare C-4 charge.

Figure 4.2 shows the shock wave vs time profiles obtained experimentally and that obtained using CTH. It is observed that the simulation results follow the same general trend as the experimental results, but the bare charge profiles obtained using the BOS method do not align with the computer simulation profile. Ideally, the experimental bare charge profiles would align with the computational profile because all profiles are scaled to 1-kg charges, and no casing was present. However, the simulation is using JWL EOS, which properties are obtained using the cylinder explosion test. This test is a good approximation up to 7 times the volume of the explosive, because iron starts to fragment beyond 7 volumes [39]. Thus, the CTH simulation is not expected to be accurate beyond 7 times the volume of the charge. For this case, the volume of the charge (625 cm^2) is obtained using the mass and the density of C-4, which results in a 7V value of 4375 cm^2. This volume corresponds to a radius of 10.14 cm, which means that an agreement between the profiles is expected 10 .14cm out of the center of the charge. Figure 4.2 shows the CTH simulation agrees with the bare curves going out a distance of almost a meter, which is well over the expected value.

For comparison purposes, the experimentally obtained Mach number profiles were also compared to the Mach number profile of the CTH simulation. The Mach numbers with respect to position for the simulation were obtained using Equation 3.1. As mentioned before, the comparison is between ideal and real

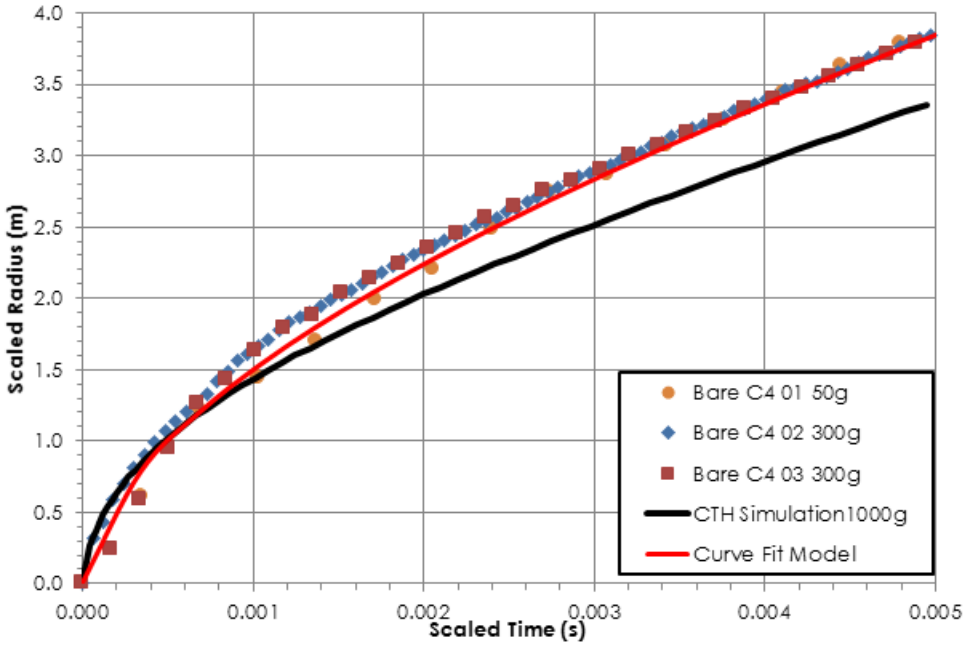

Figure 4.2: A comparison between scaled shock wave radius vs time profiles obtained experimentally and computationally.

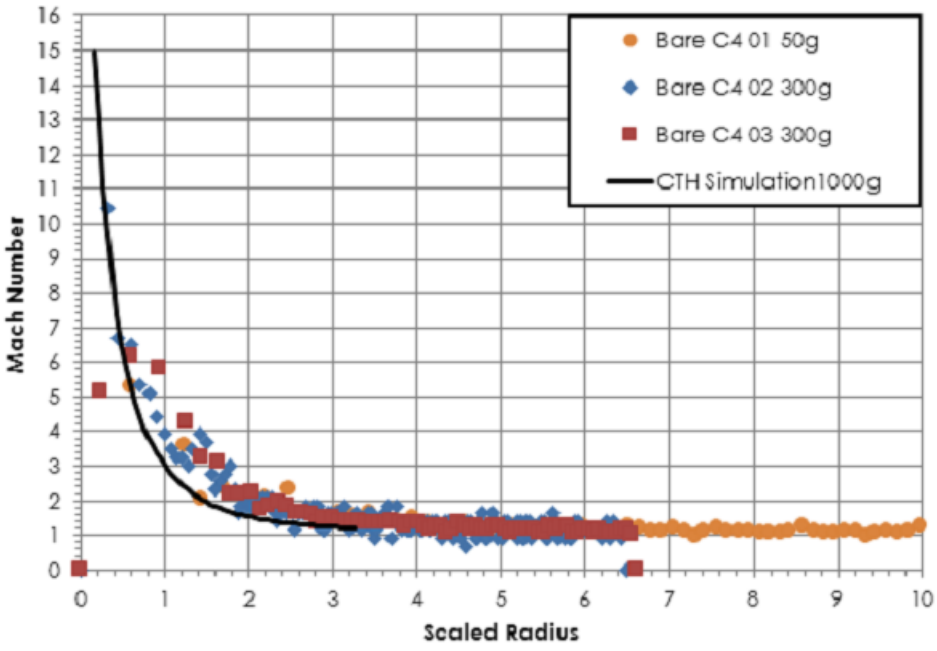

Figure 4.3: A comparison between Mach number vs scaled radii profiles obtained experimentally and computationally.

scenarios. However, Figure 4.3 shows that the experimental profiles follow the same trend obtained from the computational analysis.

Equation 3.2 was used to obtain the overpressure profile of the CTH simulation, which is shown in Figure 4.4. Again, the profiles show an agreement in trend. The difference in peak pressures between the 300-gram and the 1000-gram charges is fairly large, although both pressures are of the same magnitude. Further investigation on this discrepancy would be required, but is not included in the present work.

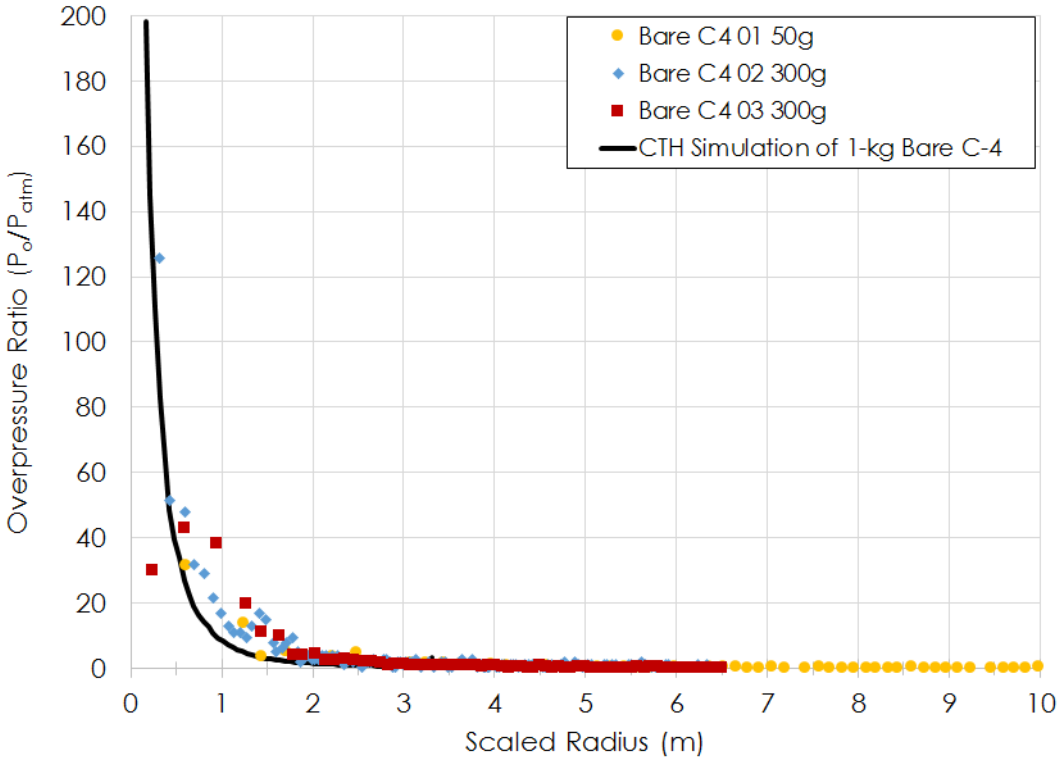

Figure 4.4: A comparison between scaled shock wave radius vs overpressure ratio profiles obtained experimentally and computationally.

CHAPTER 5

CONCLUSION AND FUTURE WORK

The background oriented schlieren was used in the present work to analyze the shock wave propagation of several encased and uncased C-4 and ANFO explosions. The shock wave location was plotted as a function of time. From these data and information of each event, such as temperature and pressure, scaled results were obtained using Sachs scaling laws. The Mach numbers were plotted as a function of the scaled radii of each explosion. From the Mach number, the overpressure was calculated. Moreover, the C-4 profiles are compared to results obtained using the CTH hydrocode developed by Sandia National Labs. These profiles are used to characterize the explosives presented in this thesis.

BOS is a technique that can accurately track the shock wave caused by the detonation of high explosives in a laboratory environment [3]. Nevertheless, the BOS method is proved to be effective when analyzing and tracking the shock wave of large-scale experiments performed outdoors, as shown in Figure 3.1. From the information gathered after applying the BOS method to the high speed images of the detonation of C-4 and ANFO, characteristic profiles for each of these explosives were obtained. These characteristic profiles helped determine, or support results in literature, of whether C-4 and ANFO could be scaled.

The scaled results obtained for Composition C-4 supported those presented by Hargather [11], and were in well agreement with the hydrocode simulations. A mass equivalence of $\mu = 0.16$ kg was obtained by scaling the bare curve fit profile to the encased curve fit profile. This indicates that a bare C-4 charge of 0.16-kg would generate the same shock wave profile as a 1-kg pipe bomb, which, based on the results presented in this thesis, is a reasonable value. This, in addition with the minimum equipment required, indicates that the BOS process can be used as a relatively cheap alternative to explosives characterizations. Future work consists on using different casing materials and investigating the energy lost due to fragmentation of such casing materials. Moreover, working with larger mass charges in similar confinement, and scaling them down to a 1-kg charge, would prove consistency with the results presented here, which were scaled up to a 1-kg charge.

The Ammonium Nitrate Fuel Oil results, although showing good agreement in their profile trends, should be complimented with more experiments. Even though the masses of the ANFO charges did not vary, the inconsistency in the casings, i.e. cars, prevented the profiles to overlap as expected. Areas of fu-

ture improvement include working with a more consistent setup by encasing the ANFO in the same material every time. By eliminating variables, one can eliminate sources of error. If it is possible, use the same kind of car (year, make, and model) to be able to compute how much energy is absorbed by the fragments and how much damage they do to the surrounding area during a car bomb explosion. Also, more high speed videos of larger masses of bare charges at different masses are required to improve scalability results.

Both C-4 and ANFO results could be improved by attempting to minimize uncertainties within the measurements. One thing that could be done is having larger pixel-to-physical calibration objects. Increasing the contrast on the area the fireball is estimated to glow would help make the identification of the pixel leading the shock wave more accurate. Also, maximizing the sensitivity of the BOS system while taking into account the constraints would help get better images, which could later be used to obtain quantitative density measurements.

CTH simulations are a good comparison to the results obtained experimentally. However, the equations of state used for the simulation (JWL) are obtained using a cylinder test, which is only accurate to 7 fold volumes. Thus, comparing physical results with computational simulation results only serves as a good theoretical estimation the closer the measurements are taken to the center of the charges. The detonation of a mass with a larger radius could be simulated to have more agreement between experimental results and computational results.

The knowledge acquired using the BOS method at a large scale could be applied to other explosives commonly used in IEDs. The results presented here could help First Responders to scientifically visualize important information regarding the explosive events. Characteristic knowledge on the shock wave created after the detonation of an improvised explosive device would help First Responders to be prepared to attend physical injuries caused by the shock wave overpressure.

Understanding the dangers involved in an IED detonation could save lives if the shock wave characteristics of the explosive are known. Thus, the information gathered in this work is useful and necessary regardless if the explosive device has been detonated or not. The findings of this work can be used to gather basic but crucial information, such as the distance where one would be safe from pressure and debris. Moreover, if the information found here is paired with structural damage knowledge, better assessments can be made by First Responders, and improvements can be made to the protective equipment provided to rescuers.

The present research has demonstrated the ability to use the BOS method to analyze explosives at a large scale. This method proved to be a cheaper, and more efficient way to characterize explosives [28] [11]. The results presented here expanded on the laboratory-scaled methods previously investigated by other researchers, as well as support data previously gathered from large scale experimentation. Information regarding the shock wave characteristics of different explosives would lead to a better understanding of how IEDs work and what could be done to minimize or eradicate the destruction they cause.

REFERENCES

[1] Hargather, M.J., Lawson, M.J., and Settles G.S. Focusing-schlieren piv measurements of a supersonic turbulent boundary layer. *47th AIAA Aerospace Sciences Meeting Including The New Horizons Forum and Aerospace Exposition*, 2009.

[2] Hargather, M.J., Settles G.S. Retroreflective shadowgraph technique for large-scale flow visualization. *Applied Optics*, 48:4449–4477, 2009.

[3] Hargather, M.J., Settles G.S. A comparison of three quantitative schlieren techniques. *Optics and Lasers in Engineering*, 50:8–17, 2011.

[4] Kleine, H., Dewey, J.M., Ohashi, K., Mizukaki, T., Takayama, K. Studies of the tnt equivalence of silver azide charges. *Shock Waves*, 13:123–138, 2003.

[5] Clarke, S.A., Bolme, C. A., Murphy, M.J., London, C.D., Mason, T.A., Adrian, R. J., Akinci, A.A., Martinez, M.E., and Thomas, K.A. Using schlieren visualization to track detonator performance. *AIP Conference Proceedings*, 955:1089, 2007.

[6] Biss, M.M., and Settles, G.S. On the use of composite charges to determine insensitive explosive material properties at the laboratory scale. *Propellants, Explosives, Pyrotechnics*, 35:452–460, 2010.

[7] Kleine, H., Timofeev, E., and Takayama, K. Laboratory-scale blast wave phenomena - optical diagnostics and applications. *Shock Waves*, 14:343–357, 2005.

[8] Klinge, F., Kirmse, T., and Kompenhans J. Application of Quantitative Background Oriented Schlieren (BOS): Investigation of a Wing Tip Vortex in a Transonic Wind Tunnel. *Proceedings of PSFVIP-4*, page F4097, 2003.

[9] Sommersel, O.K., Bjerketvedt, D., Christensen, S.O., Krest, O., Vaagsaether, K. Application of background oriented schlieren for quantitative measurements of shock waves from explosions. *Shock Waves*, 18:291–297, 2008.

[10] Hargather, M.J., Settles, G.S. Natural-background-oriented schlieren imaging. *Exp. Fluids*, 48:59–68, 2010.

[11] Hargather, M.J. Background-oriented schlieren diagnostics for large-scale explosive testing. *Shock Waves*, 23:529–536, 2013.

[12] Weapons of mass destruction training: Incident response to terrorist bombings. Print, July 2010.

[13] Kucera, J., Koch, A., and Sirak, M. US Steps Up Efforts to Counter Bomb Threats. *Jane's Defence Weekly*, page 10, October 2004.

[14] Weapons of mass destruction training: Prevention of and response to suicide bombing incidents. Print, November 2011.

[15] *NFPA 921: Guide for Fire and Explosion Investigations*. National Fire Protection Association, August 2014.

[16] Cooper, P.W. *Explosive Engineering*. Wiley - VHC, Inc., 1996.

[17] Vandersall, K.S., Switzer, L.L., and Garcia, F. Threshold studies on tnt, composition b, c-4, and anfo eexplosive using the seven impact test. *13th International Detonation Symposium*, 2006.

[18] Buczkowski, D. Detonation properties of mixtures of ammonium nitrate based fertilizers and fuels. *Central European Journal of Energetic Materials*, 8:99–106, 2011.

[19] Short, M. Quirk, J.J., Kiyanda, C.B., Jackson, S.I., Briggs, M.E., and Shinas, M.A. Simulation of detonation of ammonium nitrate fuel oil mixture confined by aluminum: Edge angels of dsd. *In Proceedings of the 14th International Detonation Symposium*, pages 769–778, 2010.

[20] Goldstein, S. Johnson, J. N. Aquarium tests on aluminized anfo. Electronic Report 2629, Los Alamos National Laboratories, Los Alamos, NM, 1981.

[21] Hargather, M.J. *Scaling, Characterization, and Application of Gram-Range Explosive Charges to Blast Testing of Materials*. Phd. thesis, Pennsylvania State University, May 2008.

[22] Hargather, M.J., and Settles G.S. Optical measurement and scaling of blasts from gram-range explosive charges. *Shock Waves*, 17:215–223, 2007.

[23] Dewey, J.M. Spherical shock waves. In Igra O. Ben-Dor, C. and E. Elperin, editors, *Handbook of Shock Waves, Vol. 2*, 2001.

[24] Sachs, R.G. The dependence of blast on ambient pressure and temperature. BRL Report 466, Ballistic Research Laboratories, May 1944.

[25] Dewey, J. M. The properties of a blast wave obtained from an analysis of the particle trajectories. *Proceedings of the Royal Society of London Series A - Mathematical and Physical Sciences*, 324:275–299, 1971.

[26] Dalziel, S.B., Hughes, G.O., Sutherland, B.R. Synthetic schlieren. In G.M. Carlomagno, editor, *Proc. 8th International Symposium on Flow Visualization*, number 62, Sorrento, Italy, 1998.

[27] G.E.A. Meier. Hintergrund schlierenmessverfahren. *Deutsche Patentanmeldung*, (DE 199 42856 A1), 1999.

[28] Meier, G.E.A. Computarized background-oriented schlieren. *Experiments in Fluids*, 33:181–187, 2002.

[29] Venkatakrishnan, L., Meier, G.E.A. Density measurements using the background oriented schlieren technique. *Experiments in Fluids*, 37:237–247, 2004.

[30] Clemedson C.J., Pettersson, H. Propagation of a high explosive air shock wave through different parts of an animal body. *American Journal of Physiology*, 184:119–126, December 1955.

[31] Mizukaki T., Wakabayashi, K., Matsumura, T., Nakayama, K. Background - oriented schlieren with natural-background for quantitative visualization-sualization of open-air explosions. *Shock Waves*, 23, 2013.

[32] Satheesh, K., Jagadeesh, G., and Reddy, K.P.J. High speed schlieren facility for visualization of flow fields in hypersonic shock tunnels. *Current Science*, 92, January 2007.

[33] Richard, H., Raffel, M. Principle and applications of the background oriented schlieren (bos) method. *Measu*, 12:1576–1585, 2001.

[34] Vision Research Inc. Phantom camera products - phantom 711, May 2014.

[35] Romero, V. Personal Interview, October 2014.

[36] Catanach, R.A., Hill, L.G. Diameter effect curve and detonation front curvature measurements for anfo. *AIP Conference Proceedings*, 620:906, June 2002.

[37] Hardstad, E. Cth shock physics, Date Accessed: April 2014.

[38] Crawford, D.A., Brundage, A.L., Harstad, E.N., Ruggirello, K., Schmitt, R.G., Schumacher, S.C., and Simmons, J.S. Cth user's manual and input instructions, February 2013.

[39] Kerley, G., and Christian-Frear, T. Prediction of explosive cylinder tests using equations of state from the panda code. Report SAND93-2131, Sadia National Laboratories, September 1993.

BACKGROUND - ORIENTED SCHLIEREN ANALYSIS OF SHOCK WAVE PROPAGATION FROM ENCASED AND UNCASED EXPLOSIVES

by

Cynthia Paulinne Romo